Structure of ^{4}Li and ^{4}He observed in the ^{1}H(α,^{3}He p)n reaction

B. Brinkmöller,* H. P. Morsch, P. Decowski,† M. Rogge, R. Siebert,‡ and P. Turek
Institut für Kernphysik, Forschungszentrum Jülich, Postfach 1913,
D-5170 Jülich, Federal Republic of Germany
(Received 12 March 1990)

Kinematically complete measurements of the ^{1}H(α,^{3}He p)n reaction at $E_\alpha = 170$ MeV were made at several ^{3}He and proton angles. Assuming an incoherent sum of different multipole contributions in different reaction channels, it was possible to describe all measured spectra consistently, taking into account sequential decay of states in ^{4}He and ^{4}Li and the p-n final state interaction. The parameters used to describe the p-n final state interaction and excited states in ^{4}He are consistent with previous measurements. Resonance energies and widths for the ground state and the first excited state of ^{4}Li were extracted which are considerably lower than assumed so far. The measured cross sections are in agreement with distorted-wave Born approximation calculations using folding form factors.

I. INTRODUCTION

The $A=4$ system is the lightest nuclear system showing a complex energy level structure.[1] Therefore it is used as a testing ground for theoretical models. (See, for instance, Refs. 2–5.)

Of special interest has been the study of isospin related properties. From a large body of photonuclear data for ^{4}He it was concluded[6] that the ratio of cross section $R=\sigma[^4\mathrm{He}(\gamma,p)t]/\sigma[^4\mathrm{He}(\gamma,n)^3\mathrm{He}]$ is ≈ 1.6 for $E_\gamma = 25$–30 MeV. This result was interpreted as evidence for strong isospin mixing between the $J^\pi=1^-$ states in ^{4}He. Recent work[7] on (γ,p) and (γ,n) indicates, however, that the cross-section ratio might be lower. Typical theoretical values are $R=1.1$ to 1.2 if only Coulomb mixing is included.[8] The strength of an additional charge symmetry breaking force needed to describe the difference in photoneutron and photoproton cross sections on ^{4}He claimed by Ref. 6 is in contradiction to other measurements.[9] Results of the isospin mixing calculations depend strongly on the wave functions used. Measurements[10] of the ^{2}H(d,p)^{3}H reaction showed evidence for a $T=0$, $J^\pi=1^-$ state at $E_x=24.1$ MeV in ^{4}He. Calculations using the Coulomb interaction as the only charge symmetry breaking force showed that the inclusion of this state increases the theoretical value of R slightly.[11] A value of $R=1.6$ could only be obtained by assuming a $J^\pi=1^-$, $T=0$ state with an energy closer to that of the $J^\pi=1^-$, $T=1$ state. However, the level scheme of the $T=1$ states in ^{4}He is not well known experimentally. This is because generally in reactions populating states in ^{4}He isoscalar excitations are dominant. Information on the $T=1$ levels in the $A=4$ system can be obtained by studying the levels in the ^{4}H and ^{4}Li mirror nuclei. These can be reached by single charge exchange reactions on ^{4}He. However, no measurements of such reactions have been reported so far.

In the case of ^{4}H several other experiments were made to extract level parameters. However, the positions and widths of the resonances extracted from these experiments differ considerably. For example, a phase-shift analysis of the elastic t-n scattering[12] gave a ground-state energy of $E_R=3.4$ MeV above the t-n threshold and a reduced width of $\gamma^2=5.5$ MeV. In the measurement of the $\pi^-+{}^6\mathrm{Li}\rightarrow{}^2\mathrm{H}+{}^4\mathrm{H}$ and the $\pi^-+{}^7\mathrm{Li}\rightarrow{}^3\mathrm{H}+{}^4\mathrm{H}$ reactions[13] peaks were found in the ^{2}H and ^{3}H spectra corresponding to resonances in ^{4}H at $E_R=5.2\pm1.5$ MeV and $E_R=8.2\pm1.5$ MeV. The analysis of the kinematically complete measurements of the ^{7}Li(π^-,tt)n reaction[14] and the ^{7}Li(n,αt)n reaction[15] led to a resonance energy $E_R=2.7\pm0.6$ MeV and a width $\gamma^2=2.3\pm0.6$ MeV for the ^{4}H ground state. Finally we note that in a missing mass measurement of the ^{9}Be(^{11}B, ^{16}O)^{4}H reaction a resonance energy of 3.5 ± 0.5 MeV was found.[16]

The only source of information on ^{4}Li states until now are phase-shift analyses of the ^{3}He-p elastic scattering, which were reported by several authors.[17–20] Tombrello[17] found a level ordering of $J^\pi=2^-$, 1^- (triplet), 0^-, 1^- (singlet) with an energy $E_R=4.7$ MeV above the ^{3}He-p threshold for the 2^- ground state, $E_R=6.2$ MeV for the 1^- first excited state and widths of $\gamma^2=5.5$ MeV for both these states. These results were later questioned by Morrow and Haeberli.[19] More recent results[20] for the analyzing power of the ^{3}He-p elastic scattering confirmed the level ordering, but the energies and widths differed substantially from the old values.

It is therefore important to get information on ^{4}Li from other reactions. The kinematically complete measurement of the (p,n) reaction with inverse kinematics ^{1}H(α,^{3}He p)n is well suited for such an investigation. The production cross section of ^{4}Li in this reaction can be compared with DWBA calculations for single-particle charge exchange. Contributions from four-body final states can be excluded. Due to the inverse kinematics a large center of mass solid angle can be covered even with small detectors.

II. EXPERIMENTAL SETUP

The experiment was performed using a momentum analyzed α beam from the Jülich cyclotron with an energy $E_\alpha = 170$ MeV. A 10-μm-thick Mylar foil was used as a target. The hydrogen content of this foil is 4.2% giving a thickness of 58.4 μg/cm^2. This was checked by comparing the cross section of the ^{1}H(α,^{3}He)d reaction with values from the literature.[21,22] The results agreed within 10%. The large enhancement in the center-of-mass solid angle for the ^{1}H(α,^{3}He p)n reaction made it possible to measure this reaction with only little background. Even spectra taken on a 1.4-μg/cm^2 hydrogen impurity of a lead target could be used for the analysis.

A velocity diagram for the final state of the reaction $p+\alpha \rightarrow {}^4\text{Li}+n \rightarrow {}^3\text{He}+p+n$ is shown in Fig. 1. The relationship of the measured quantities $v_{\text{lab}}(^3\text{He})$, $v_{\text{lab}}(p)$, $\Theta_{\text{lab}}(^3\text{He})$, and $\Theta_{\text{lab}}(p)$ to the quantities used for the theoretical description of this reaction, can be deduced from this diagram. These variables are (i) the scattering angle $\Theta_{\text{c.m.}}$ of the primary reaction, (ii) the angle Φ between the ^{4}Li recoil direction and the direction of the proton emission for the sequential decay $^4\text{Li} \rightarrow {}^3\text{He}+p$, and (iii) the relative velocity v_{rel} and thereby the energy E_{rel} of the sequential decay.

To be able to measure the $p(\alpha,^4\text{Li})n$ reaction under a small angle $\Theta_{\text{c.m.}}$ by using the decay of $^4\text{Li} \rightarrow {}^3\text{He}+p$ the detectors for the ^{3}He and the proton have to be set up at opposite sides of the beam. Small relative angles between ^{3}He and p correspond to small relative energies $E_{\text{rel}}(^3\text{He},p)$. In our experiment the protons were measured using two ΔE-E telescopes consisting of a 1-mm silicon ΔE detector and a 14-mm high purity germanium E detector mounted under a fixed relative angle of 12° in a cryostat. The ^{3}He's were measured with a 1-mm silicon ΔE detector and an 8-mm silicon E detector, consisting of four 2-mm detectors which were selected to operate with the same high voltage.

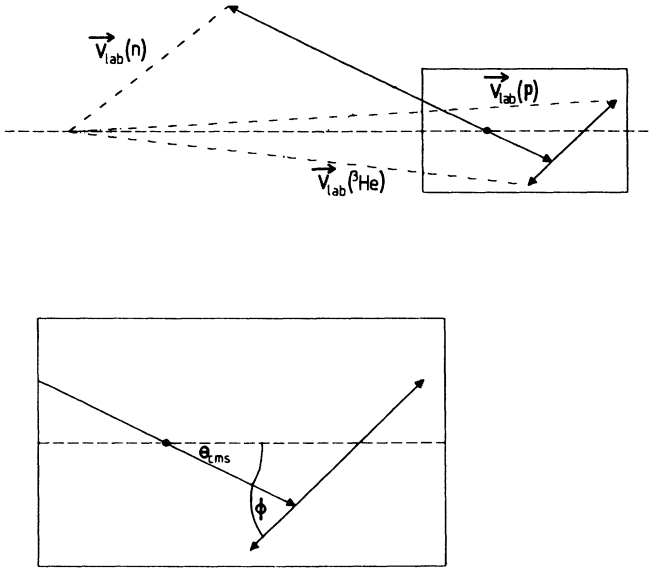

FIG. 1. Velocity diagram of the $p+{}^4\text{He} \rightarrow n+{}^4\text{Li}$ reaction with subsequent decay $^4\text{Li} \rightarrow {}^3\text{He}+p$. The velocities in the center-of-mass system and the laboratory system are shown together with the angles $\Theta_{\text{c.m.}}$ and Φ which are explained in the text. The relative energy $E_{\text{rel}}(^3\text{He},p)$ can be calculated from $v_{\text{rel}}(^3\text{He},\text{p})$.

III. DISCUSSION OF THE DATA

A. General considerations

A Dalitz plot of the ^{1}H(α,^{3}He p)n reaction of the phase-space section defined by $\Theta_{\text{lab}}(^3\text{He}) = 10.5°$ and $\Theta_{\text{lab}}(p) = -14.5°$ is shown in Fig. 2. The kinematically

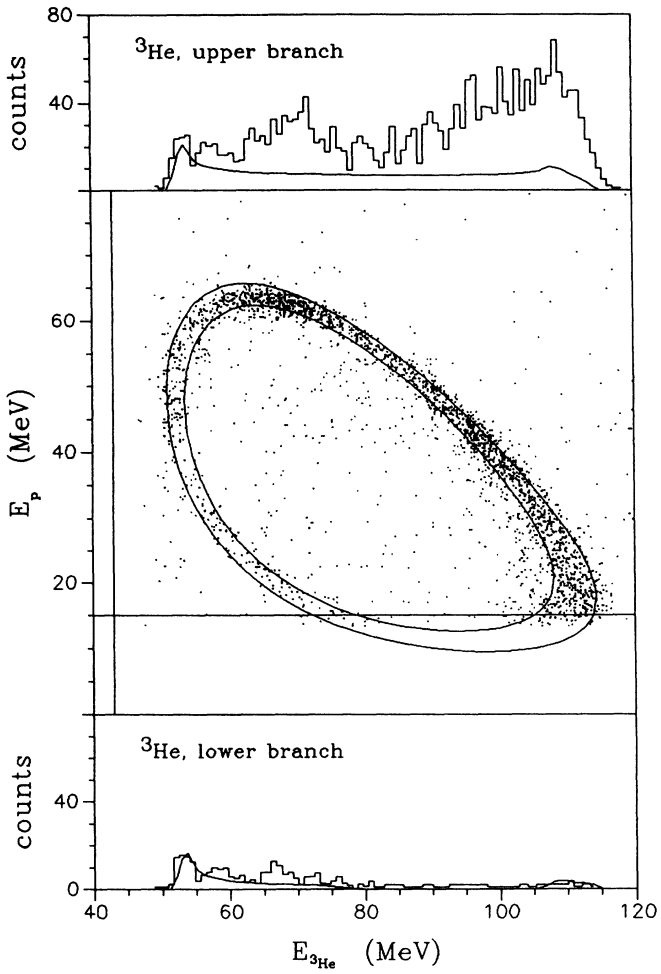

FIG. 2. Dalitz plot of the $p({}^4\text{He}, {}^3\text{He},p)n$ reaction of the phase-space section defined by a detector setting of Θ_{lab} (^{3}He) = 10.5° and $\Theta_{\text{lab}}(p) = -14.5°$. The limits of the detector acceptance are indicated by the straight lines in the two-dimensional plot. The calculated kinematical allowed region is given by the curved lines. Projections of the upper and lower branches of the kinematic locus on the $E_{^3\text{He}}$ axis together with three-body phase-space calculations are also shown.

allowed region given by the angular acceptance of the detectors is clearly seen. This kinematic locus is well reproduced by calculations (curved solid lines), giving a good check for the energy and angle calibrations.

Above and below the two-dimensional plot are projections of the upper and lower branches of the kinematic locus on the $E(^3\mathrm{He})$ axis. These spectra are compared to results of phase-space calculations which were fitted to the data to estimate the largest possible three-body phase-space contribution to the cross section. Especially for the upper branch the experimental yield exceeds this phase-space contribution considerably. This additional yield has to be due to quasifree processes and/or processes with sequential breakup.

In the $^1\mathrm{H}(\alpha,^3\mathrm{He}\,p)n$ reaction studied here the only quasifree process that may contribute is the break-up of the α particle. The quasifree cross section peaks at $\Theta(^3\mathrm{He})=0°$ with a decrease toward larger angles.[23] For a fixed angle $\Theta(^3\mathrm{He})$ the dependence on $\Theta(p)$ resembles that of a $p(n,n)p$ reaction. These characteristics of breakup reactions could not be observed in the data. It can be concluded that quasifree processes do not contribute significantly. This reduces the discussion to three different sequential processes:

$p+\alpha\rightarrow{}^3\mathrm{He}+p,n$ with proton-neutron final-state interaction ,

$p+\alpha\rightarrow p+{}^4\mathrm{He}^*$ with sequential decay ${}^4\mathrm{He}^*\rightarrow{}^3\mathrm{He}+n$,

$p+\alpha\rightarrow n+{}^4\mathrm{Li}^*$ with sequential decay ${}^4\mathrm{Li}^*\rightarrow{}^3\mathrm{He}+p$.

Figure 3 shows the kinematically allowed region together with the region in which events with a ^{3}He-p relative energy of 4.7 MeV (the ^{4}Li ground-state energy according to Ref. 17) occur for the spectrum shown in Fig. 2. The width of the calculated regions is due to the angular acceptance of the detectors. Contributions from ^{4}Li ground-state decay can be expected to be strong where the two regions overlap (dashed areas). The angle $\Theta_{\mathrm{c.m.}}$ (^{4}Li) of the primary $p(\alpha,{}^4\mathrm{Li})$n reaction which is given in the figure is quite different at the three overlap regions.

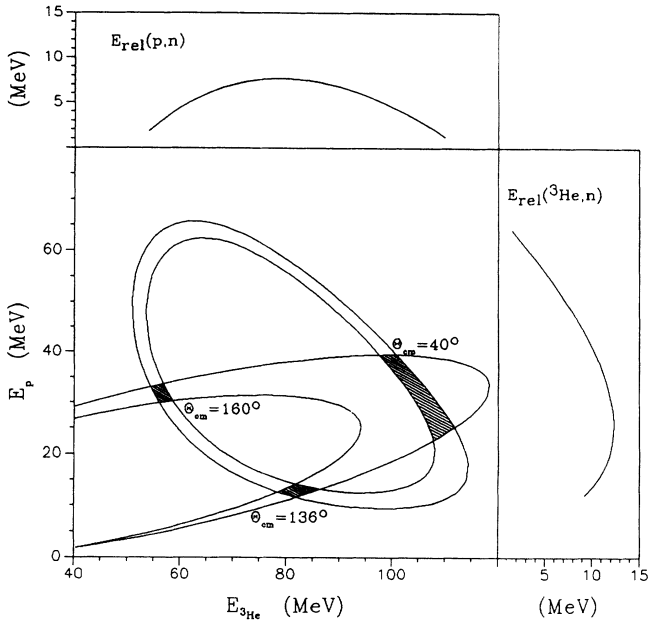

FIG. 3. Kinematically allowed region of the spectrum shown in Fig. 2 overlaid with the region corresponding to a relative energy $E_{\mathrm{rel}}(^3\mathrm{He},p)=4.7$ MeV. The widths of these regions are given by the angular acceptance of the detectors. Decay of ^{4}Li states with $E_{\mathrm{rel}}(^3\mathrm{He},\mathrm{p})=4.7$ MeV contributes to the shaded overlap regions. For each of the overlap regions the angle $\Theta_{\mathrm{c.m.}}$ for the primary $p(\alpha,{}^4\mathrm{Li})$n reaction is given. Above the two-dimensional plot $E_{\mathrm{rel}}(p,n)$ as a function of $E_{^3\mathrm{He}}$ and to the right $E_{\mathrm{rel}}(^3\mathrm{He},\mathrm{n})$ as a function of E_p is given.

The relative energies of the p-n system E_{rel} (p-n) a a function of $E(^3\mathrm{He})$ were calculated for the center of the detectors and are shown at the top of Fig. 3. The cross sections for the p-n final-state interaction peaks at small $E_{\mathrm{rel}}(p$-$n)$. This process contributes mainly at the minimal and maximal ^{3}He energy to the cross section.

$E_{\mathrm{rel}}(^3\mathrm{He}$-$n)$ is shown at the right of Fig. 3. Structure due to the decay of states in ^{4}He is only expected at small E_{rel} (^{3}He-n). Due to the low center-of-mass energy of $E_{\mathrm{c.m.}}=34$ MeV and the Q value (-20 MeV) of the reaction studied here, the cross section for formation of intermediate states in ^{4}He with high excitation energies is further reduced. DWBA calculations show that the cross section decreases linear with increasing excitation energy. Therefore it is unlikely to see excited states at large E_{rel} and the decay of ^{4}He contributes mainly at the maximal possible proton energy.

So it is possible to study the effects of each process separately. This may justify an analysis of the data in which the contributions of the different processes are added incoherently.

B. Theoretical cross sections

The cross section σ at a point of the phase space for any sequential process depends on the resonance form $f_1(E_{\mathrm{rel}})$ of the intermediate state and the angular distribution $f_3(\Theta_{\mathrm{c.m.}})$ of the primary reaction forming the resonance. Further the decay angular distribution $f_2(\Phi)$ has to be considered. The decay pattern is in general a function of $\Theta_{\mathrm{c.m.}}$ as well. However, for all spectra measured in this experiment the angle $\Theta_{\mathrm{c.m.}}$ for the reaction leading to resonant states in ^{4}He and ^{4}Li is nearly constant. So the cross section can be written as

$$\sigma=C\rho f_1(E_{\mathrm{rel}})f_2(\Phi)f_3(\Theta_{\mathrm{c.m.}}) , \tag{3.1}$$

where ρ is the phase-space factor and C a normalization constant.

The data were analyzed by comparing calculated spectra with the measured spectra. To obtain the theoretical spectra the function in Eq. (3.1) was integrated over the phase-space region covered by the angular acceptance of the detectors using a Monte Carlo program[24] for each possible sequential process. Where possible, resonance forms $f_1(E_{\rm rel})$ and angular distributions $f_2(\Phi)$ and $f_3(\Theta_{\rm c.m.})$ for the p-n final-state interaction and the sequential decay of states in ^{4}He and in ^{4}Li were taken from previous experiments or theoretical calculations. Parameters that could not be fixed this way were varied until a good description of the data was obtained. For each set of parameters the normalization constants C in Eq. (3.1) were fitted to optimize the description of the experimental data by the sum of the theoretical spectra. Spectra measured at different angles were fitted simultaneously using the same set of normalization constants. The following sections describe the parameters used for the calculation of the contributions of the different processes to obtain a consistent description of the data.

1. The p-n final-state interaction

The proton-neutron final-state interaction is well known and was measured in several experiments. Watson and Migdal[25,26] found that the cross section for the production of a proton and a neutron with small relative energy $E_{\rm rel}$ as a function of the relative momentum of the pair is proportional to the phase space ρ times the square of the proton-neutron scattering wave function. The latter depends on $E_{\rm rel}$ and it follows:[27]

$$\sigma_{s,t} \sim \rho \frac{(1/r_{s,t}+1/a_{s,t}+\frac{1}{2}r_{s,t}k^2)^2}{k^2+(1/a_{s,t}+\frac{1}{2}r_{s,t}k^2)^2} , \qquad (3.2)$$

where k is the wave number of the proton-neutron relative motion, $r_{s,t}$ is the effective range, and $a_{s,t}$ the scattering length of the singlet and triplet scattering, respectively. With the values[28] $a_s=-23.68$ fm, $r_s=2.5$ fm, $a_t=5.40$ fm, and $r_t=1.7$ fm one obtains the cross section by taking the incoherent sum of the singlet and triplet contributions: $\sigma=\sigma_s+3\sigma_t$.

The angular distribution $f_2(\Phi)$ for the decay has to be isotropic, as only the proton-neutron s wave contributes. The angular distribution of the primary reaction $f_3(\Theta_{\rm c.m.})$ follows closely the angular distribution of the $p(\alpha,{}^3{\rm He})d$ reaction.[21,22] So all parameters needed to describe the proton-neutron final-state interaction are well known and one can calculate the contribution of this process to the spectra.

2. States in ^{4}He

In the spectrum taken at $\Theta_{\rm lab}(^3{\rm He}) = 11.2°$, $\Theta_{\rm lab}(p)=-16.0°$ (Fig. 4) one can see a peak at $E_{^3{\rm He}}\approx 70$ MeV. This peak is due to the decay of the $T=1$, $J^\pi=2^-$ state in ^{4}He with a relative energy $E_{\rm rel}$ (^{3}He-n)≈ 1.5 MeV. To describe this peak the resonance form $F_1[E_{\rm rel}(^3{\rm He}\text{-}n)]$ was extracted from pion scattering experiments[29] on ^{4}He. For a given state the dependence of the measured cross section $\sigma_{\alpha(\pi,\pi')}$ on the relative energy $E_{\rm rel}(^3{\rm He}\text{-}n)$ is different from the energy dependence in our experiment as the available phase space is different. In addition the decrease of the cross section in our reaction with increasing $E_{\rm rel}(^3{\rm He}\text{-}n)$ predicted by DWBA calculations cannot be seen in the pion data. The function $f_1[E_{\rm rel}(^3{\rm He}\text{-}n)]$ was corrected to account for these differences.

The angular distribution $f_2(\Phi)$ of the decay of this state has a large influence on the measured spectra. As this state is formed by an $s\rightarrow p$ transition, the angular distribution of its decay is determined by the wave function of the nucleon in the p shell. From spherical har-

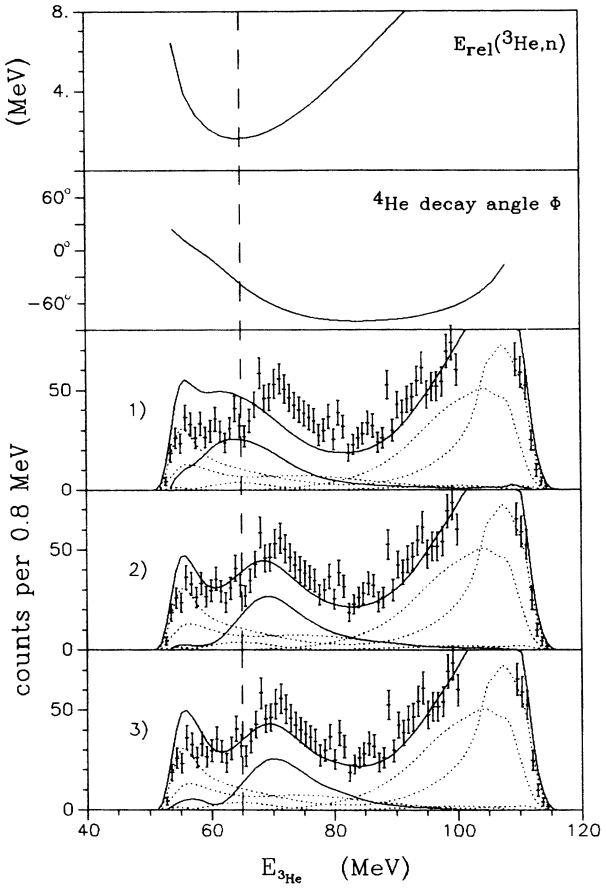

FIG. 4. Example of different fits to a spectrum at $\Theta_{\rm lab}(^3{\rm He})=11.2°$ and $\Theta_{\rm lab}(p)=-16.0°$ to show the effect of the angular distribution of the decay of the $J^\pi=2^-$ state in ^{4}He. In the upper part $E_{\rm rel}(^3{\rm He,n})$ and the ^{4}He decay angle Φ are shown as a function of $E_{^3{\rm He}}$. The vertical dashed line indicates the position in the spectra where the cross section for exciting the 2^- state peaks [$E_{\rm rel}(^3{\rm He})\approx 1.5$ MeV]. In the lower three parts the contributions of this state calculated using different assumption for the decay angular distribution are shown as solid lines (see the text). Also shown by a solid line is the sum of all channels. The contributions of channels which are not discussed here are indicated by dotted lines. They can be identified by referring to Fig. 11 which shows the same spectrum.

monic functions it follows that a p-shell nucleon can be emitted with a $f_2(\Phi)=c_1+c_2\sin^2(\Phi+\Phi_0)$ distribution, where the constants depend on the occupation of the subshells.

In Fig. 4 fits with different assumptions for $f_2(\Phi)$ are shown. The spectrum generated with an isotropic distribution gives a peak centered at the minimum of the ^{3}He-n relative energy (spectrum 1 in Fig. 4). This is not consistent with the peak in the experimental spectrum which is shifted toward higher ^{3}He energies. A similar behavior was already seen in previous measurements of the $\alpha(p,^3\text{He}\ p)n$ reaction.[30] This can be explained by a unisotropic decay.

Use of a $f_2(\Phi)=\sin^2\Phi$ distribution with respect to the ^{4}He recoil direction describes the measurements much better (spectrum 2 in Fig. 4). However, the calculated maximum is still shifted slightly in comparison with the measured peak. The best fit is obtained with a distribution $f_2(\Phi)=\sin^2(\Phi+10°)$ (spectrum 3 in Fig. 4). Thus, the decay pattern has a maximum nearly perpendicular to the recoil axis.

The angular distribution $f_3[\Theta_{\text{c.m.}}(^4\text{He}^*)]$ for the primary reaction was taken from DWBA calculations (Sec. IV). For all spectra measured in this experiment the angle $\Theta_{\text{c.m.}}(^4\text{He}^*)$ was $\approx 140°$. This angle changes only slightly along the kinematic locus so that the angular distribution $f_3[\Theta_{\text{c.m.}}(^4\text{He}^*)]$ has only little influence on the results of the fit.

Besides the 2^- state other higher lying states in ^{4}He contribute to the cross section, with the largest contribution coming from the $J^\pi=1^-$, $L=1$ state. However, no clear structure due to this state was found in this experiment. To estimate the contribution of the higher lying states in ^{4}He to the background, calculations with a resonance form derived from inelastic pion scattering to the 1^- state[29] were made. The pion cross section was not divided by the appropriate phase-space factor so that the maximum of the resonance is shifted to higher $E_{\text{rel}}(^3\text{He}$-$n)$. In this way the influence of all higher lying states ^{4}He was taken into account approximatively. The contribution of this state to the cross section is small in all spectra. The experimental data are not inconsistent with an isotropic decay of this state, however, a $f_2(\Phi)=1+\sin^2\Phi$ distribution was used in the fits, as such a distribution described the decay of the 1^- state of ^{4}Li best (see data discussed in Sec. III C). The angular distribution $f_3=\Theta_{\text{c.m.}}(^4\text{He}^*)$ was taken from DWBA calculations for an $L=1$ angular momentum transfer.

In one spectrum (Fig. 5) measured at Θ_{lab} (^{3}He)$=10.4°$ and Θ_{lab} (p)$=-23°$, the kinematic locus includes phase-space regions with very small $E_{\text{rel}}(^3\text{He}$-$n)$. Using only the ^{4}He states discussed so far, the cross section is underestimated in the region of $E_{^3\text{He}}\approx 70$ MeV. In analogy to the well-known p-t final-state interaction,[31-32] ($0^+,\alpha^*$) one might observe a similar effect above the $n+^3$He threshold. Assuming such an $n+^3$He final-state interaction the spectrum in Fig. 5 is well described. The additional peak is narrower than that of the p-t final-state interaction because of the missing Coulomb repulsion. Unfortunately, the contribution of this interesting 0^+ state is seen only in one spectrum. Further, the fit depends strongly on the decay angular distribution of the neighboring 2^- state. For example, a small isotropic component for the decay of this state would fill up part of the minimum at $E_{^3\text{He}}\approx 70$ MeV. Therefore, the parameters describing the 0^+ state have large uncertainties.

C. States in ^{4}Li

The contribution of the decay of ^{4}Li states is clearly seen on the upper and lower branches of the kinematic locus in many spectra. The resonance form f_1 [$E_{\text{rel}}(^3\text{He}$-$p)$] extracted from the data is influenced strongly by assumptions about the angular distribution $f_2(\Phi)$ of the ^{4}Li decay. However, we found that use of the resonance parameters extracted from phase-shift analyses of the ^{3}He-p elastic scattering for the ^{4}Li ground state[17] cannot describe the data.

The resonance form is given by[14,33]

$$f_1(E_{\text{rel}})=\frac{P\gamma^2}{(E_R-\gamma^2 S-E)^2+P^2\gamma^4}\ , \tag{3.3}$$

with

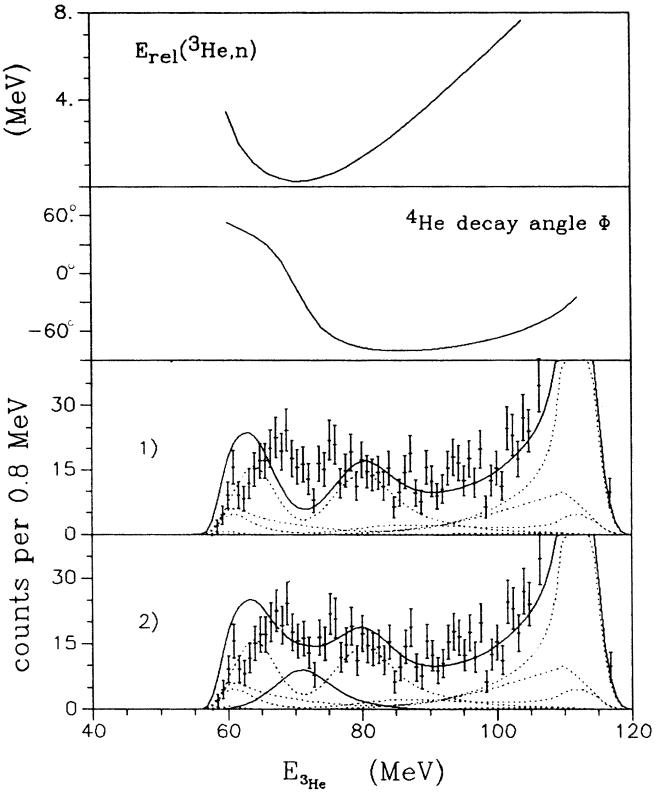

FIG. 5. Example of different fits to a spectrum at $\Theta_{\text{lab}}(^3\text{He})=10.4°$ and $\Theta_{\text{lab}}(p)=-23.0°$ to show the effect of the inclusion of the ^{3}He-n final-state interaction. The description is similar to that of Fig. 4. The solid line in the lower part gives the contribution of the 0^+ state in ^{4}He. The contribution from the other channels can be identified by referring to Fig. 12.

$$S=kr\frac{FF'+GG'}{F^2+G^2},\quad P=kr/(F^2+G^2)\ ,$$

where F and G are the regular and irregular solutions of the Coulomb equation calculated at a channel radius of 4 fm, that was used to describe the ^{3}He-p elastic scattering.[17]

Using this formula and the resonance parameters $E_R=4.7$ MeV, $\gamma^2=5.5$ MeV, and assuming isotropic decay of ^{4}Li one gets a very broad distribution (spectrum 1 in Fig. 6). The description of the data is improved if an angular distribution $f(\Phi)=\sin^2(\Phi+\Phi_0)$ for the decay is used (spectrum 2 in Fig. 6). Nevertheless, one obtains only one broad maximum, whereas our experimental spectra indicate two more narrow structures. A good description can be obtained by assuming two states with smaller resonance energies E_R and smaller width γ^2. The best fit to the data gave $E_R=3.3$ MeV and $\gamma^2=1.0$ MeV for the ground state and $E_R=5.9$ MeV, $\gamma^2=1.5$ MeV for the first excited state (spectrum 3 in Fig. 6).

Because the energy of the ground state of ^{4}Li was found to be much lower than expected its decay contributes significantly only to the spectrum measured at the smallest ^{3}He-p relative angle in this experiment. Here it has to be emphasized that the necessity of introducing two distinct resonances does not arise alone from the spectrum shown in Fig. 6 but from a consistent fit to all the spectra measured, for example, of the spectrum in Fig. 7 where only the higher lying state is seen.

The resonance parameters for the ^{4}Li ground state were obtained using a $f(\Phi)=\sin^2(\Phi-10°)$ decay distribution. An equally good description could be obtained using $\gamma^2=0.5$ MeV and $f(\Phi)=\sin^2\Phi$ for this state. So, the width γ^2 and the angle Φ_0 are only roughly determined. The similarity of the decay pattern of this state with the $J^\pi=2^-$ state in ^{4}He suggests a 2^- assignment for this state as well. This is consistent with theoretical expectations.[1]

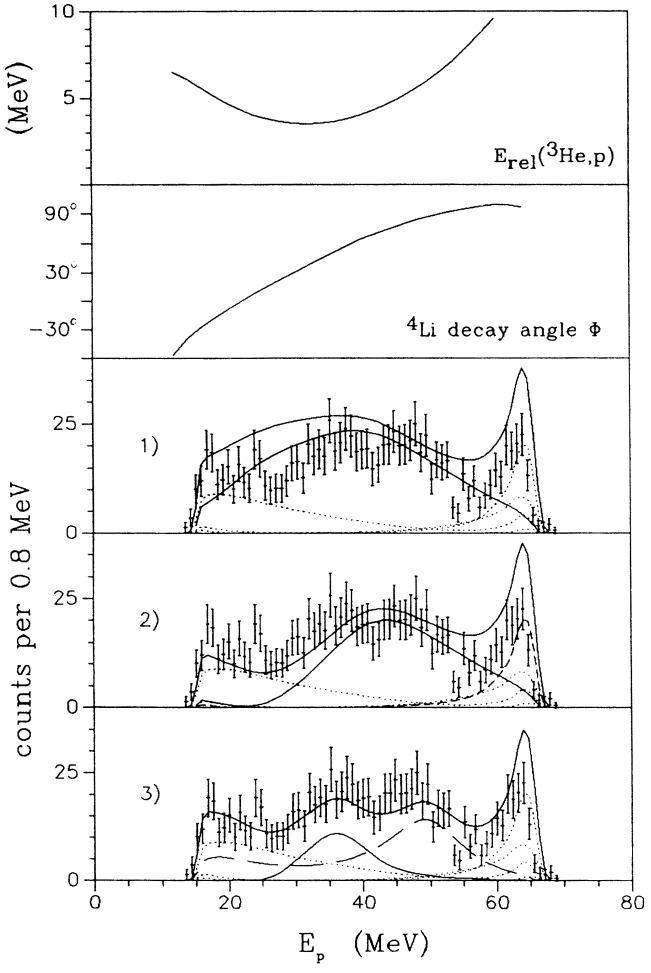

FIG. 6. Example of different fits to a spectrum at $\Theta_{lab}(^3\text{He})=10.4°$ and $\Theta_{lab}(p)=-11.0°$ to show the effect of different fits for states in ^{4}Li. The description is similar to that of Fig. 4. The solid line in the three lower parts of the plot gives the contribution of the 2^- state and the dashed line the contribution of the 1^- state in ^{4}Li. The relevant variables now are $E_{rel}(^3\text{He},p)$ and the ^{4}Li decay angle Φ. The contribution from the other channels can be identified by referring to Fig. 8.

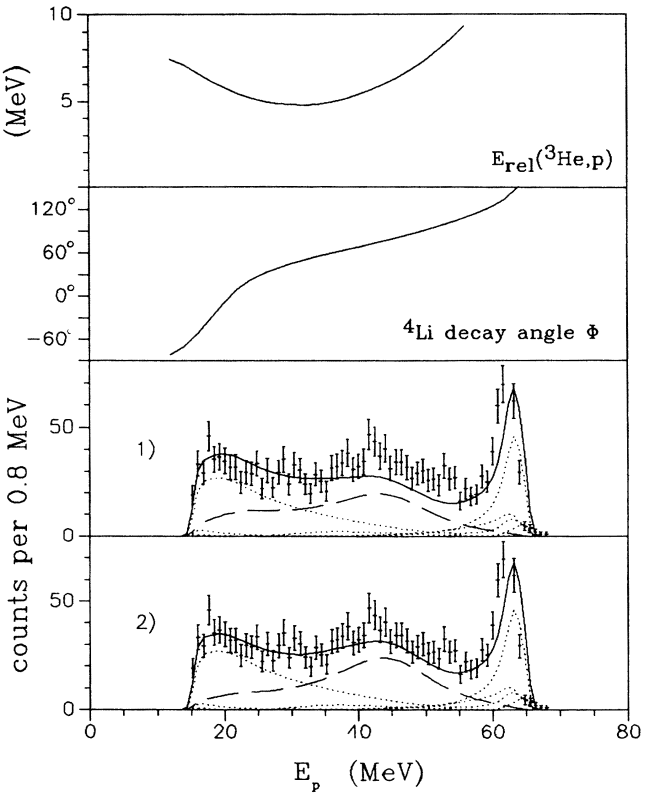

FIG. 7. Example of different fits to a spectrum at $\Theta_{lab}(^3\text{He})=10.5°$ and $\Theta_{lab}(p)=-14.5°$ to show the effect of the angular distribution of the decay of the $J^\pi=1^-$ state in ^{4}Li. The description is similar to that of Fig. 6. The dashed line in the lower two parts gives the contribution of this state. The contribution from other channels can be identified by referring to Fig. 9.

TABLE I. Summary of parameters used to describe the resonance form f_1, the decay angular distribution f_2, and the angular distribution f_3 of the primary reaction for the states used in the analysis.

State	$f_1(E_{rel})$	$f_2(\Phi)$	$f_3(\Theta)$
pn	Ref. 27	Isotropic	Refs. 21 and 22
$\alpha(2^-)$	Ref. 29	$\sin^2(\phi+\phi_0)$	DWBA calculations
$\alpha(1^-)$	Ref. 29	$1+\sin^2\phi$	DWBA calculations
^{4}Li(2^-)	$E_r=3.3$ MeV, $\gamma^2=1.0$ MeV	$\sin^2(\phi+\phi_0)$	DWBA calculations
^{4}Li(1^-)	$E_r=5.9$ MeV, $\gamma^2=1.5$ MeV	$1+\sin^2\phi$	DWBA calculations

The first excited state of ^{4}Li was observed under several different kinematic conditions. The yield for this state may be described using an isotropic decay (spectrum 1 in Fig. 7). However the fit is improved slightly, when a $f_2(\Phi)=1+\sin^2\Phi$ distribution is used (spectrum 2 in Fig. 7). From phase-shift analyses and theoretical calculations it follows, that this state has spin and parity of $J^\pi=1^-$. Because of the larger number of combinations possible for the coupling of $L=1$, $S=1$ to a 1^- state the angular distribution should be more isotropic, consistent

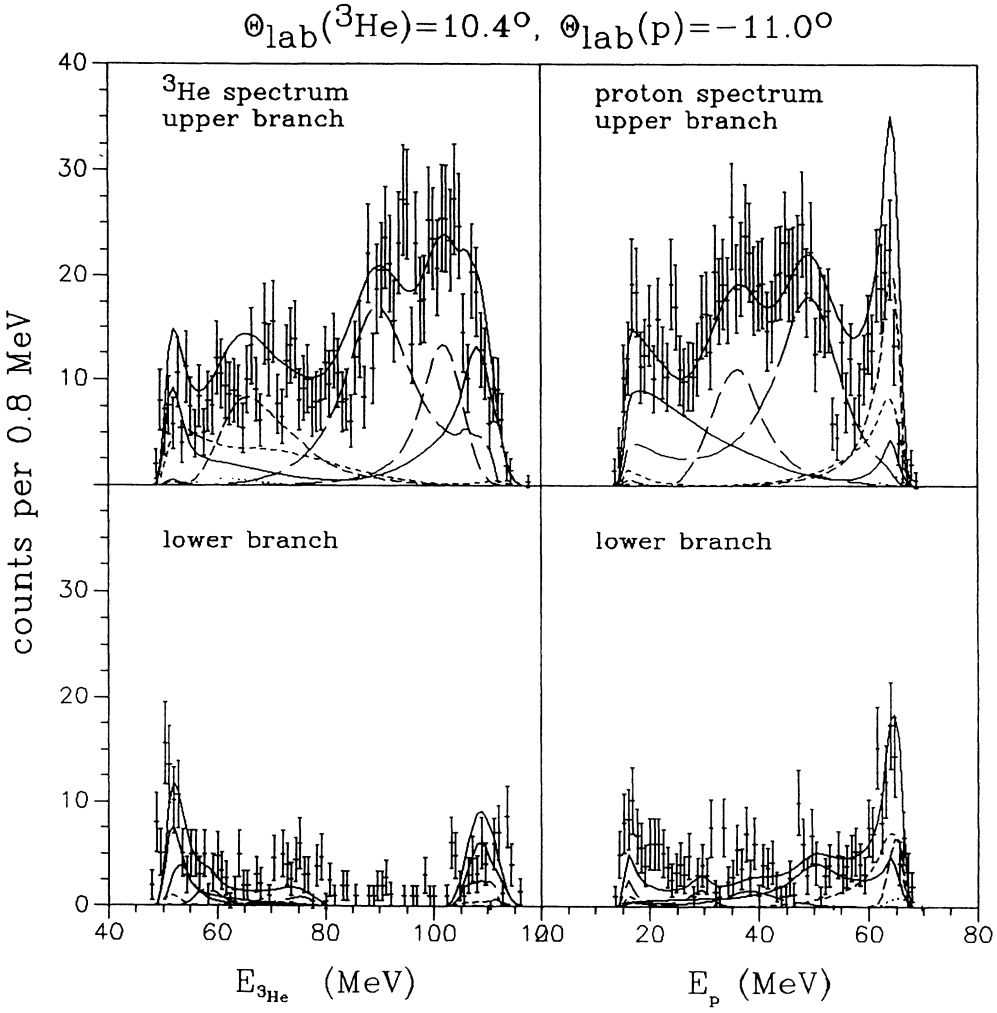

FIG. 8. Projections of the upper and lower branches on the $E_{^3\mathrm{He}}$ and E_p axis for an experimental spectrum. The different curves show the calculated contributions of different states to the spectrum. *p-n* final-state interaction—solid lines. 0^+ state in ^{4}He—dotted lines. 2^- state in ^{4}He—short dashed lines. 1^- state in ^{4}He—very short dashed lines. 2^- state in ^{4}Li—long dashed lines. 1^- state in ^{4}Li—very long dashed lines.

with our observation.

On the upper branch of the kinematic locus ^{4}Li is seen with small $\Theta_{c.m.}(^4\text{Li})$ whereas on the lower branch $\Theta_{c.m.}(^4\text{Li})$ is large (Fig. 3). Therefore the angular distribution of the primary reaction is essential for the ratio of cross sections on these branches. The angular distributions calculated in the DWBA (Sec. IV) describe the ratio of cross sections on the upper and lower branches quite well.

D. Summary of experimental results

In Figs. 8–12 the fits to all measured spectra are shown, sorted according to increasing relative angle $\Theta_{rel}(^3\text{He-}p)$. Projections of the ^{3}He-p coincidence spectra on both the $E_{^3\text{He}}$ and on the E_p axis are shown, as some features can only be seen in one or the other projection.

As was discussed above, the sensitivity to ^{4}Li decay with small $E_{rel}(^3\text{He-}p)$ is decreasing with increasing $\Theta_{rel}(^3\text{He-}p)$, so that the ^{4}Li ground state contributes significantly only in the spectrum measured at $\Theta_{rel}(^3\text{He-}p)=21.4°$ on the upper branch of the kinematic locus (Fig. 8). In the spectrum measured at $\Theta_{rel}(^3\text{He-}p)=33.4°$ contribution to the cross section is small for all ^{4}Li states (Fig. 12).

The description of the data is generally good. There are quite large differences between data and calculated distributions at the minimal and maximal energies in each spectrum [e.g., the ^{3}He spectra at $E(^3\text{He})\approx 110$ MeV in Fig. 12]. These are due to uncertainties in placing the cut between upper and lower branches of the kinematic locus. However, the corresponding phase-space regions are much more sensitively described in the spectra of the other particle. As the descriptions of these spectra in the relevant energy region are good [e.g., the upper branch of the proton spectrum at $E(p)\approx 20$ MeV in Fig. 12], all the cross sections are satisfactorily described.

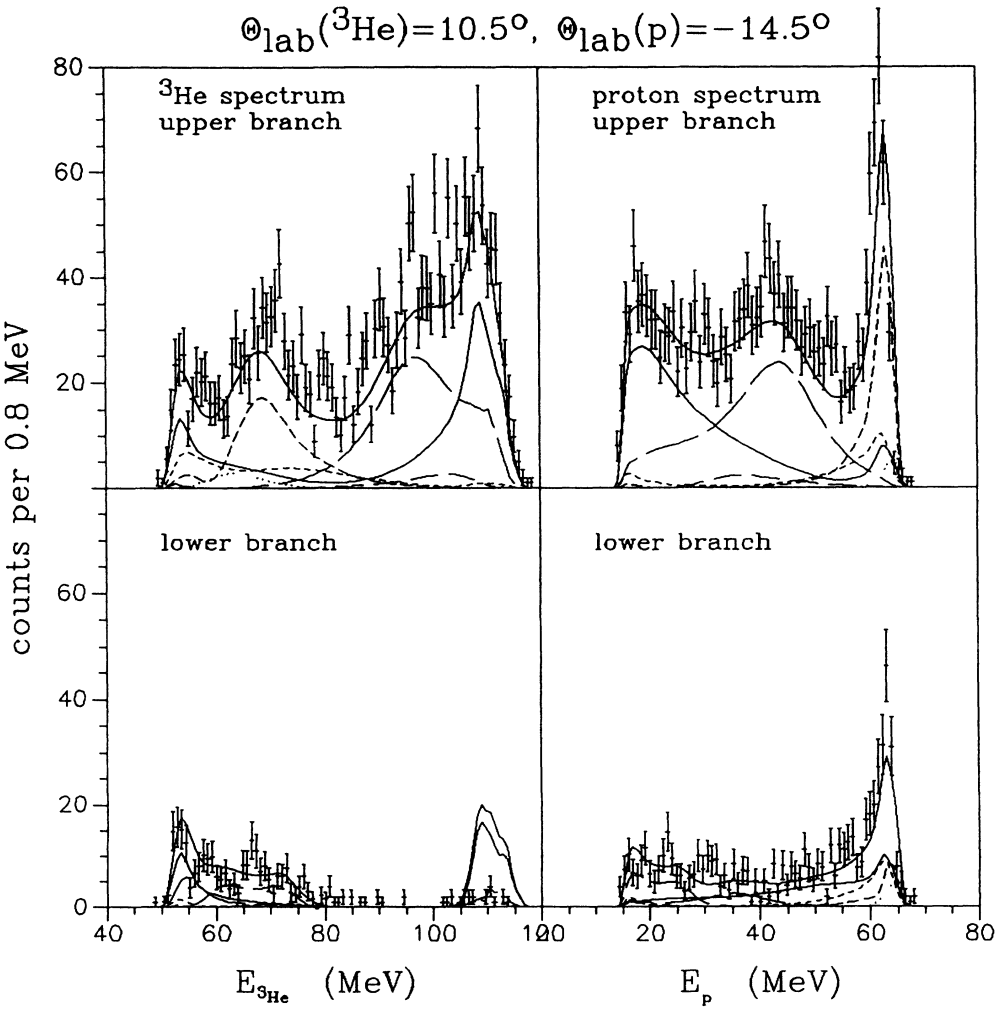

FIG. 9. Same as Fig. 8 for different angle setting.

In Table I the best fit parameters are summarized. It is possible to deduce cross sections for each process by integrating the function in Eq. (3.1) over the whole phase space. This procedure has of course large uncertainties, as the validity of the parameters in Table I was only tested for a limited number of angle settings. Different assumptions for the angular distributions of the decay $f_2(\Phi)$ or the primary reaction $f_3(\Theta_{\text{c.m.}})$ were found to change the extracted cross section up to 40% for some of the states without changing the quality of the description of the measured spectra. The largest uncertainties exist for the states in the α particle as they were only measured with large $\Theta_{\text{c.m.}}$.

In the case of the p-n final-state interaction a different normalization constant had to be used at two angles. This may be due to uncertainties in the angle setting of the detectors; a change of 0.1° in the position of a detector gives a change of 0.1 MeV in the p-n relative energy. As the cross section of this process falls off fast with increasing $E_{\text{rel}}(p\text{-}n)$, uncertainties of $\pm 0.3°$ in the position of the detectors give the observed deviation of $\pm 30\%$ for the normalization constant. The mean value of $\sigma_{p\text{-}n} = 0.53$ mb/sr found for the p-n final-state interaction is in excellent agreement with values extracted from the $\alpha(p,{}^3\text{He})pn$ reaction.[21,22]

Figure 13 shows the total cross section extracted for states in ^{4}He populated in $^4\text{He}(p,p')$ with subsequent decay into the ^{3}He-n channel and the total cross section extracted for states in ^{4}Li populated in $^4\text{He}(p,n)$. The fall-off of the cross section at higher excitation energies is influenced strongly by the limited free energy of ≈ 14 MeV available in the three-body final state. For ^{4}He the 2^- and 1^- distributions are consistent with other data.[29] In addition, the dotted line gives our estimate of the yield of the n-^{3}He final-state peak.

For ^{4}Li the resonance energies and widths of the 2^- ground state and the 1^- first excited state are much smaller than the resonance energies and widths found in ^{3}He-p elastic scattering.[17] Because the experimental cross section for the excitation of these states was not integrat-

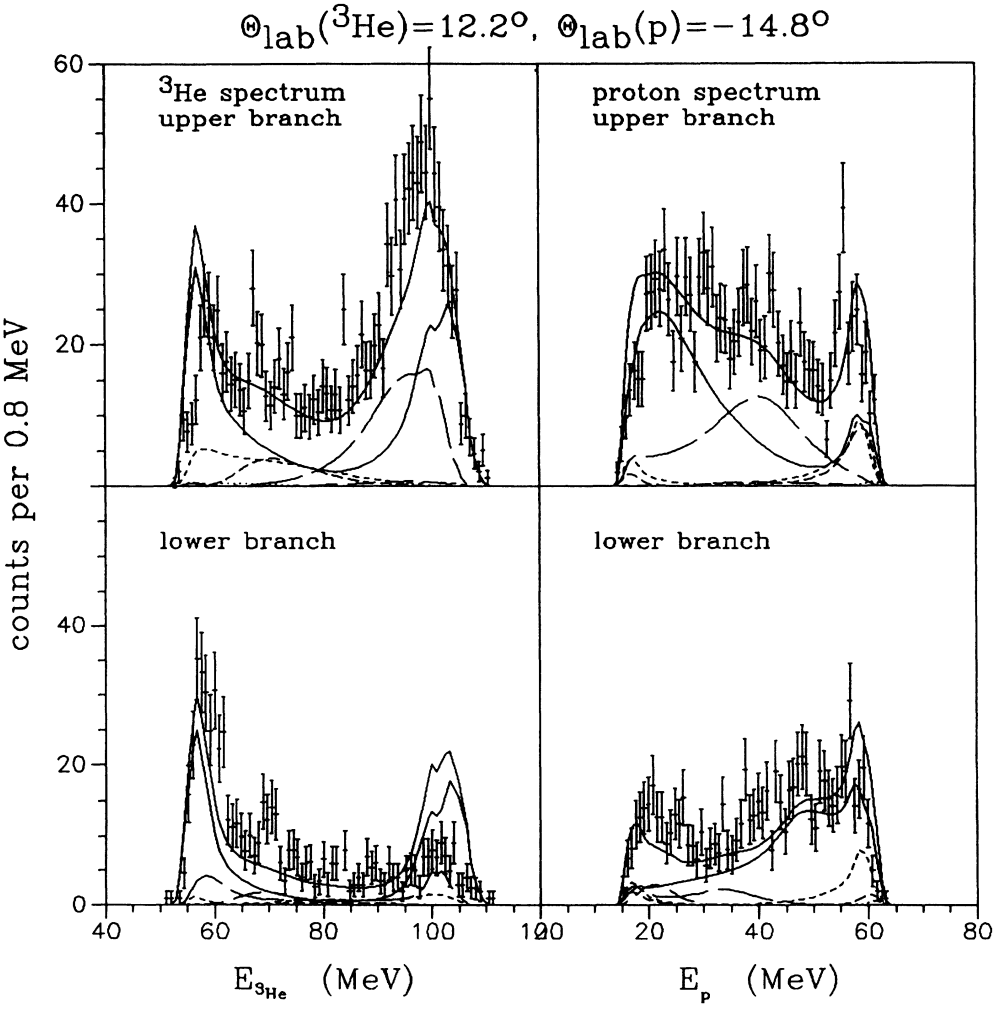

FIG. 10. Same as Fig. 8 for different angle setting.

ed over the whole decay angular distribution, interference between the 1^- and the 2^- states is possible. This interference was neglected in the analysis. However, it is unlikely that this can explain the large deviation for the level parameters observed.

IV. DWBA CALCULATIONS

The angular distributions $f_3(\Theta_{c.m.})$ of the ^{4}He(p,p') and the ^{4}He(p,n) reaction were calculated in a microscopic DWBA using folding form factors[34] for the $s \rightarrow p$ transition as discussed below.

The recoil corrected wave function u_s used to describe the s-state nucleons was calculated using a Woods-Saxon potential with a radius of $R = \sqrt{3} \times 1.25$ fm for the real and spin-orbit part. The depth of the spin-orbit potential was fixed at 6 MeV and the depth of the real part was chosen to reproduce the binding energy of $B_x = 20.5$ MeV.

As a nucleon in a p state of the $A = 4$ system is not bound, it is not possible to calculate a wave function u_p for this state in the way described for the s state. Therefore different types of wave functions were used.

1. Harmonic oscillator wave function. The parameters of the potential were chosen so that the 1s-wave function reproduced the rms radius of the α particle of ≈ 1.45 fm. The rms radius obtained for the p-wave function was 1.87 fm.

2. Unbound wave function taken from calculations of the elastic ^{3}He-p scattering. To obtain a normalization, the scattering wave function was cut at the first node. For calculations of ^{3}He-p elastic scattering at 5 MeV the wave function has a very large rms radius of about 5.4 fm. As the first node is pushed to larger radii as the ^{3}He-p energy decreases the rms radius obtained for the wave function is even larger for smaller ^{3}He-p energies.

3. Resonant wave function. Here it is assumed that ^{4}Li can only be formed, when the wave functions of ^{3}He and the proton overlap (proximity approximation). As a

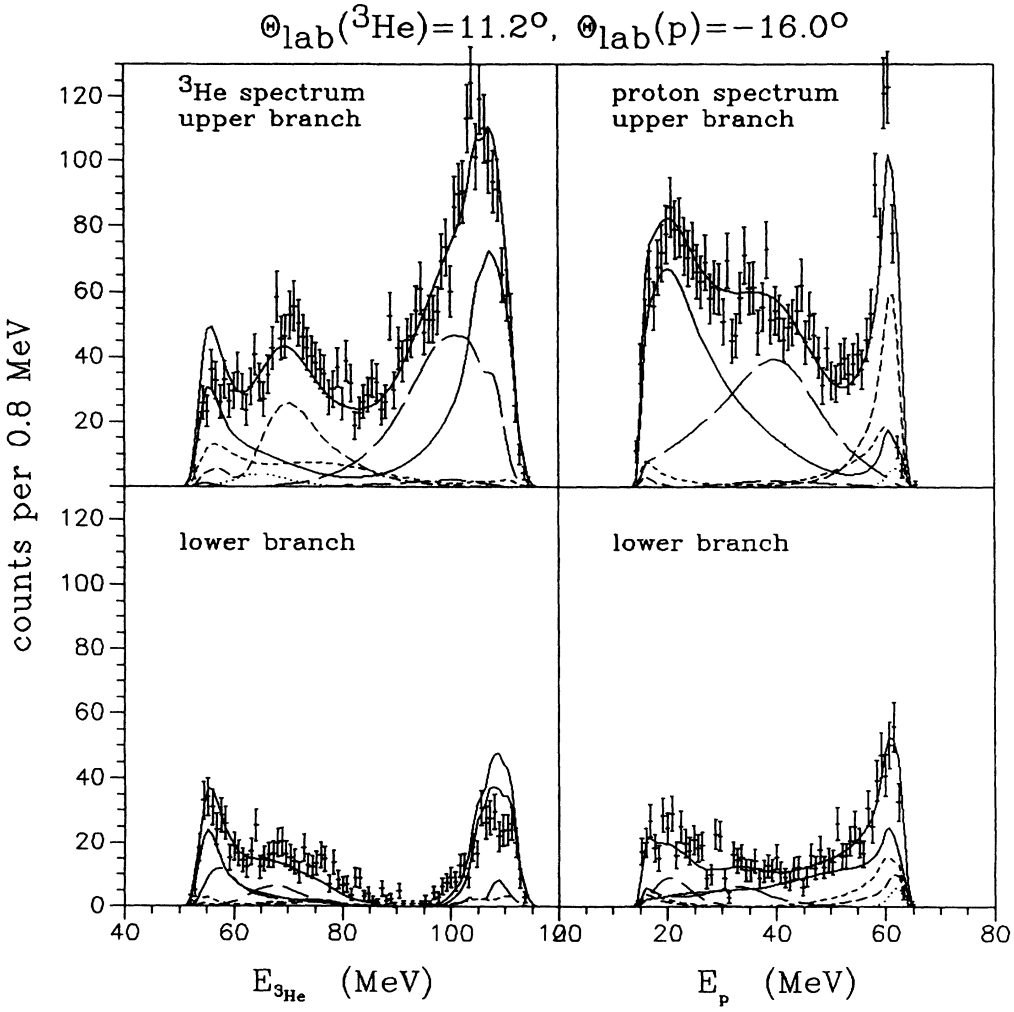

FIG. 11. Same as Fig. 8 for different angle setting.

realistic value for the rms radius of the p-state wave function one can assume the sum of the rms radii of ^{3}He (1.65 fm) and the proton (0.8 fm). A wave function with such an rms radius of 2.47 fm was obtained by folding an unbound wave function (as described in Sec. III B 2) with a Gaussian cut off. A similar wave function was used for ^{4}He.

Using such wave functions for u_p a form factor $F(r)$ was calculated with an effective nucleon-nucleon interaction $v(\mathbf{r}-\mathbf{r}_i)$; here $\mathbf{r}$ is the distance between projectile and target center of mass and $\mathbf{r}_i$ is the position of the ith target nucleon. For the effective interaction a Gaussian shape with a range of 1.68 fm was used:

$$F(r)=V_S^T\int v(|\mathbf{r}-\mathbf{r}_i|)u_s(\mathbf{r}_i)u_p(\mathbf{r}_i)r_i^2dr_i\ . \tag{4.1}$$

The depth of the interaction potential of $V_0=16.9$ MeV, $V_0^1=8.7$ MeV, $V_1^0=7.0$ MeV, and $V_1^1=7.1$ MeV was taken from a potential family that has been applied successfully to different scattering systems.[34,35]

Similarly, folding potentials were obtained for the description of the entrance and exit channels using the formula

$$U_{\rm opt}(r)=4V_0\int v(|\mathbf{r}-\mathbf{r}_i|)u_s^2(\mathbf{r}_i)r_i^2dr_i \tag{4.2}$$

for the entrance and

$$U_{\rm opt}(r)=3V_0\int v(|\mathbf{r}-\mathbf{r}_i|)u_s^2(\mathbf{r}_i)r_i^2dr_i + V_0\int v(|\mathbf{r}-\mathbf{r}_i|)u_p^2(\mathbf{r}_i)r_i^2dr_i \tag{4.3}$$

for the exit channel.

For the entrance channel the procedure could be checked by comparing measurements of the elastic p-α scattering at $E_p=31$ MeV (Ref. 36) with calculations obtained with potentials given by Eq. (4.2) (solid line in Fig. 14). At forward angles the calculated cross section describes the data quite well. Only the first minimum at $\approx 10°$ is too low in the calculation. For larger angles the calculation underestimates the cross section. This is ex-

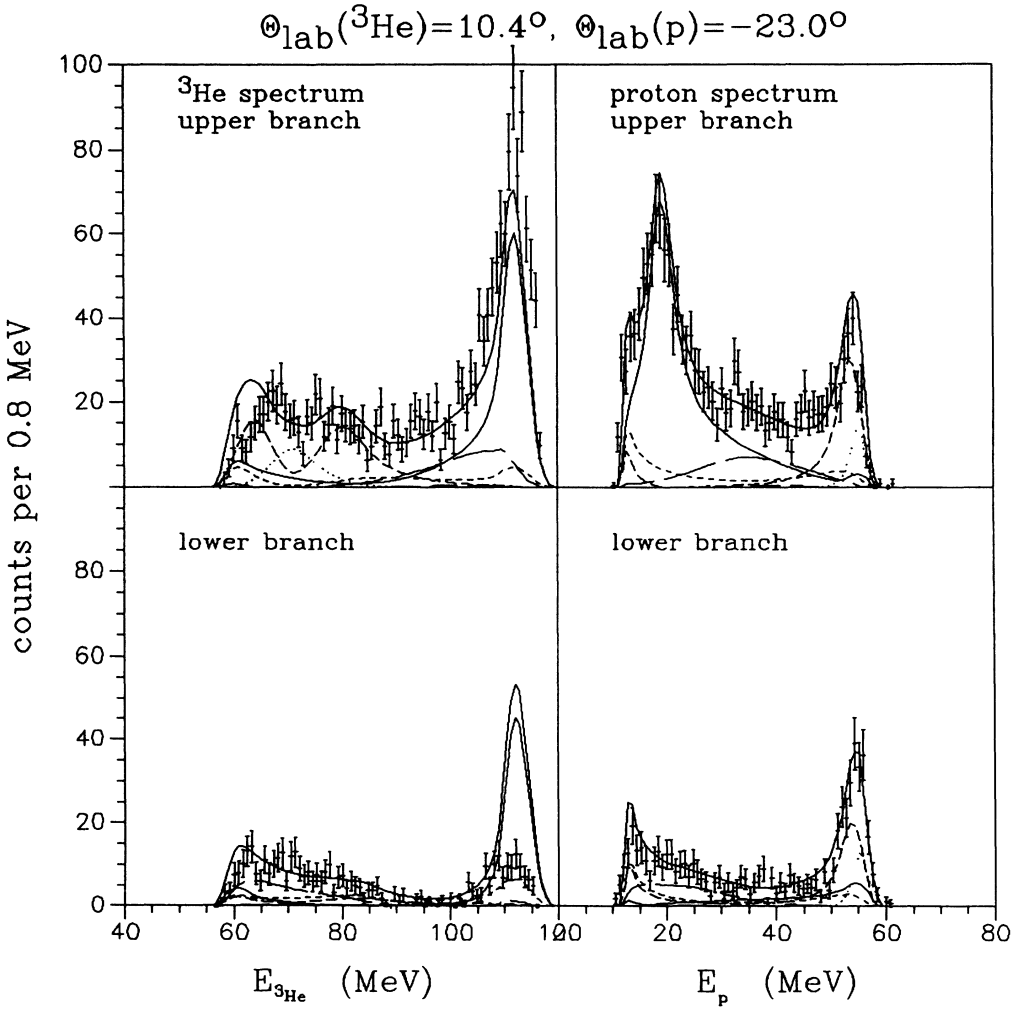

FIG. 12. Same as Fig. 8 for different angle setting.

TABLE II. Comparison of the cross section σ_{theo} calculated with DWBA and the measured cross section σ_{exp}. For the ^{4}Li(1^-) state the first number for σ_{theo} gives the cross section for the triplet state only, the number in parentheses the sum of triplet and singlet cross section.

State	σ_{theo}(mb/sr)	σ_{exp}(mb/sr)
$\alpha(2^-)$	0.95	0.72
$\alpha(1^-)$	0.27	0.34
^{4}Li(2^-)	0.26	0.18
^{4}Li(1^-)	0.14 (0.55)	0.36

pected since exchange terms were not included in our calculation.

Calculations were also performed using a complex effective interaction. Here the imaginary potential part was adjusted to fit the forward angle ^{3}He-p elastic scattering. A reasonable description could be obtained only by changing the real part of the potential to $V_0=20$ MeV with an imaginary potential depth $V_i=5$ MeV (dashed line in Fig. 14). This gives a good fit to the forward angle data; however, the dropoff of the cross section to large angles is too large.

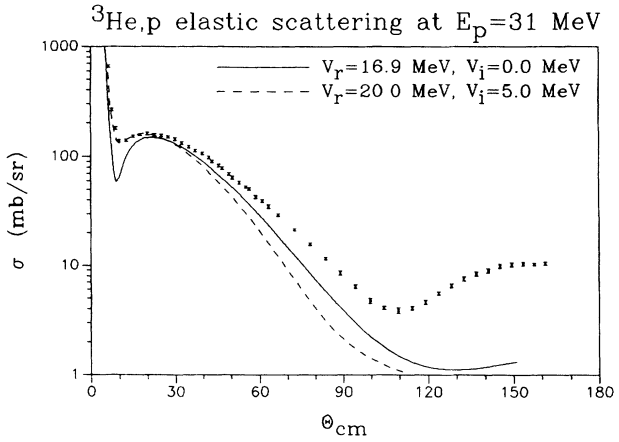

FIG. 14. Comparison of the angular distribution of the elastic ^{3}He+p scattering with optical model calculations using the folding type potentials described in the text.

Figure 15 shows the results of the ^{4}Li calculations. It was found that the shape of the angular distribution is nearly independent from the assumptions for the wave functions and the effective interaction. However, the absolute cross section decreases strongly with increasing rms radius of the p-state wave function. Further, the introduction of an absorbitive imaginary potential also reduces the cross section.

For the calculation with the real effective interaction (used in many systems[34,35]) and an rms radius of 2.47 fm for the p-state wave function, which appeared to be most realistic, absolute cross sections for different $L=1$ excitations in ^{4}He and ^{4}Li are compared to the experimental data in Table II. The value given for the 1^- states refers to the triplet state, in case of ^{4}Li also the sum of triplet and singlet states is given.

For the states in ^{4}He two decay channels are open. Be-

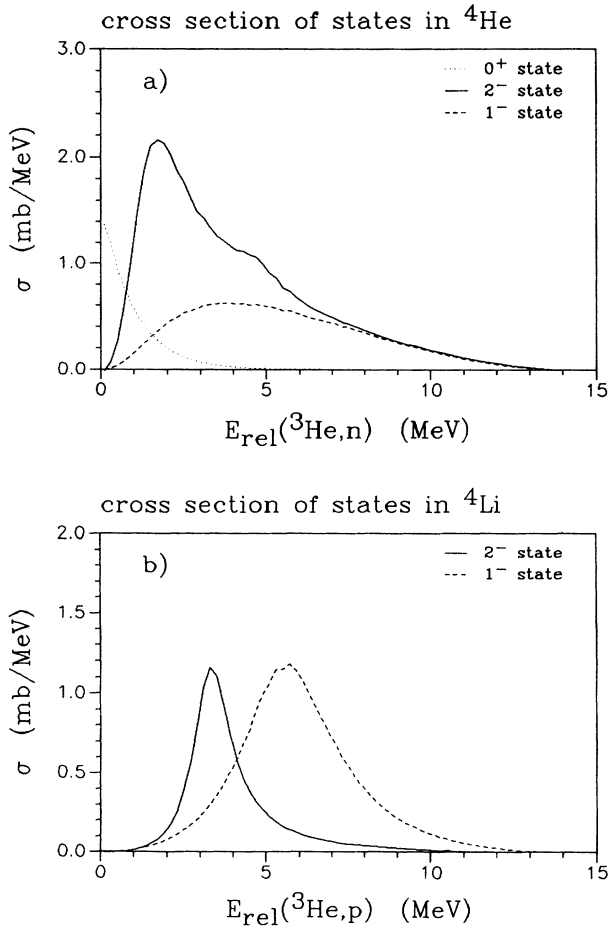

FIG. 13. (a) Cross section of the states in ^{4}He as a function of $E_{rel}(^3He,n)$. (b) Cross section of the states in ^{4}Li as a function of $E_{rel}(^3He,p)$.

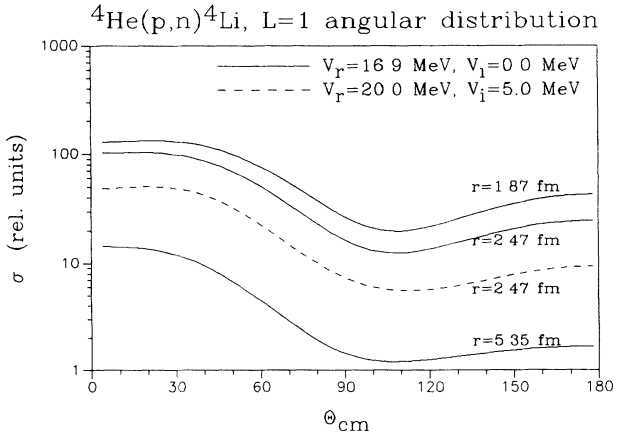

FIG. 15. $L=1$ angular distribution for the ^{4}He(p,n)^{4}Li reaction using different assumptions for the p-state wave function and the effective interaction as described in the text.

side the ^{3}He-n channel measured here, this state may also decay into the p-t channel. So, experimentally only about half of the cross section is seen. Considering this, the experimental cross section for states in ^{4}He is larger than expected, while the experimental cross section for ^{4}Li is smaller. This can be explained if a slightly larger radius for the p-state wave function in ^{4}Li is assumed than in ^{4}He. This might be due to the larger Coulomb repulsion. Considering the larger uncertainty in both the experimental and theoretical values the agreement is good.

V. CONCLUSION

In this paper we report the first measurement of the (p,n) charge exchange reaction on ^{4}He populating levels in ^{4}Li using a kinematically complete measurement of the $p(\alpha,{}^3\text{He}\ p)n$ reaction. Whereas the level parameter of states in ^{4}He and the p-n final-state interaction that are observed in the same reaction, are consistent with previous results, we find level energies and reduced widths for ^{4}Li states, that are considerably lower than assumed so far.

The cross sections for the ^{4}He(p,p') ^{4}He* and ^{4}He(p,n) ^{4}Li reactions are compared to folding model DWBA calculations. Within the experimental and theoretical uncertainties the full particle-hole strength is seen for both ^{4}He and ^{4}Li. This shows that our results for these nuclei are compatible with each other and support the ^{4}Li level parameters extracted from this experiment.

However uncertainties remain because of the low center-of-mass energy available for the reaction which limits the possibility to observe structure at higher excitation energies and because of the dependence of the extracted level parameters on assumptions made about the decay angular distribution of the resonant states. A direct measurement of the neutron in the ^{4}He(p,n) ^{4}Li reaction at intermediate proton energies would eliminate these uncertainties.

---

*Present address: University of MN, Minneapolis, MN 55455.
† Present address: Department of Nuclear Physics, Utrecht, The Netherlands.
‡Present address: Institut de Physique Nucleaire, F-91406 Orsay CEDEX, France.

[1]S. Fiarman and W. E. Meyerhof, Nucl. Phys. **A206**, 1 (1973).
[2]H. H. Hackenbroich and P. Heiss, Z. Phys. **242**, 352 (1971).
[3]D. Halderson and R. J. Philpott, Nucl. Phys. **A321**, 295 (1979).
[4]J. J. Bevelacqa, Can. J. Phys. **58**, 1555 (1980).
[5]A. M. Badalyan, T. I. Belova, N. B. Konyukova, and V. D. Efros, Sov. J. Nucl. Phys. **41**, 926 (1985).
[6]J. R. Calarco, B. L. Berman, and T. W. Donnelly, Phys. Rev. C **27**, 1866 (1983).
[7]R. Bernabei, A. Chisholm, S. d'Angelo, M. P. De Pascale, P. Picozza, C. Schaerf, P. Belli, L. Casano, A. Incicchitti, D. Prosperi, and B. Girolami, Phys. Rev. C **38**, 1990 (1988).
[8]F. C. Barker, Aust. J. Phys. **33**, 583 (1984).
[9]D. Halderson and R. J. Philpott, Phys. Rev. C **28**, 1000 (1983).
[10]W. Grübler, V. König, P. A. Schmelzbach, B. Jenny, and J. Vybiral, Nucl. Phys. **A369**, 381 (1981).
[11]J. J. Bevelaqua Phys. Rev. C **27**, 2417 (1983).
[12]T. A. Tombrello, Phys. Rev. **143**, 772 (1966).
[13]R. C. Cohen, A. D. Kanaris, S. Margilies, and J. L. Rosen, Phys. Rev. Lett. **14**, 242 (1965).
[14]U. Sennhauser, L. Felawka, T. Kozlowski, H. K. Walter, F. W. Schlepuetz, R. Engfer, E. A. Hermes, P. Heusi, H. P. Isaak, H. S. Pruys, A. Zglinski, and W. H. A. Hesseling, Phys. Lett. **103B**, 409 (1981).
[15]D. Miljanic, S. Blagus, and M. Zadro, Phys. Rev. C **33**, 2204 (1986).
[16]A. V. Belozyorov, C. Borcea, Z. Dlouhy, A. M. Kalinin, R. Kalpahchieva, Nguyen Hoai Chau, Yu. Ts. Oganessian, and Yu. E. Penionzhkevich, Nucl. Phys. **A460**, 352 (1986).
[17]T. A. Tombrello, Phys. Rev. **138**, B40 (1965).
[18]L. Drigo and G. Pisent, Nuovo Cimento **51B**, 419 (1967).
[19]L. Morrow and W. Haeberli, Nucl. Phys. **A126**, 225 (1969).
[20]R. Detomo Jr., H. W. Clark, L. J. Dries, J. L. Regner, and T. R. Donoghue, Nucl. Phys. **A313**, 269 (1979).
[21]J. G. Rogers, J. M. Cameron, M. B. Epstein, G. Paic, P. Tomas, J. R. Richardson, J. W. Verba, and P. Doherty, Nucl. Phys. **A136**, 433 (1969).
[22]S. A. Harbison, R. J. Griffiths, N. M. Stewart, A. R. Johnston, and G. T. A. Squire, Nucl. Phys. **A152**, 503 (1970).
[23]R. Siebert, H. P. Morsch, P. Decowski, M. Rogge, and P. Turek, Phys. Lett. **159B**, 95 (1985).
[24]B. Brinkmöller, thesis, University Bonn, 1987.
[25]M. Watson, Phys. Rev. **88**, 1163 (1952).
[26]A. B. Migdal, Sov. Phys. JETP **1**, 2 (1955).
[27]C. Zupancic, Rev. Mod. Phys. **37**, 330 (1965).
[28]P. A. Assimakopoulos, E. Beardsworth, P. D. Body, and P. F. Donovan, Nucl. Phys. **A144**, 272 (1970).
[29]C. L. Blilie, D. Dehnhard, D. B. Holtkamp, S. J. Seestrom-Morris, S. K. Nanda, W. B. Cottingame, D. Halderson, C. L. Morris, C. F. Moore, P. A. Seidl, H. Ohnuma, and K. Maeda, Phys. Rev. **80**, 543 (1986).
[30]J. G. Rogers, G. Paic, J. R. Richardson, and J. W. Verba Phys. Rev. C **2**, 828 (1970).
[31]R. Jahn, D. P. Stahel, G. J. Wozniak, J. Cerny, and H. P. Morsch, Phys. Lett. **65B**, 339 (1976).
[32]R. Kamermans, H. P. Morsch, R. J. de Meijer, and J. v. Driel, Nucl. Phys. **A314**, 37 (1979).
[33]A. M. Lane and R. G. Thomas, Rev. Mod. Phys. **30**, 257 (1958).
[34]H. P. Morsch, C. Sükösd, M. Rogge, P. Turek, H. Machner, and C. Mayer-Böricke, Phys. Rev. C **22**, 489 (1980), and references therein.
[35]I. Reichstein and Y. C. Tang, Nucl. Phys. **A139**, 144 (1969).
[36]S. M. Bunch, H. H. Forster, and C. C. Kim, Nucl. Phys. **B9**, 568 (1969).